LBL-22840
Preprint c.2

Lawrence Berkeley Laboratory
UNIVERSITY OF CALIFORNIA

RECEIVED
LAWRENCE
BERKELEY LABORATORY
MAR 2 1987
LIBRARY AND
DOCUMENTS SECTION

Engineering Division

To be submitted for publication

DESCRIPTION OF BEAM POSITION MONITOR SIGNALS WITH HARMONIC FUNCTIONS AND THEIR TAYLOR SERIES EXPANSIONS

K. Halbach

January 1987

TWO-WEEK LOAN COPY
This is a Library Circulating Copy
which may be borrowed for two weeks.

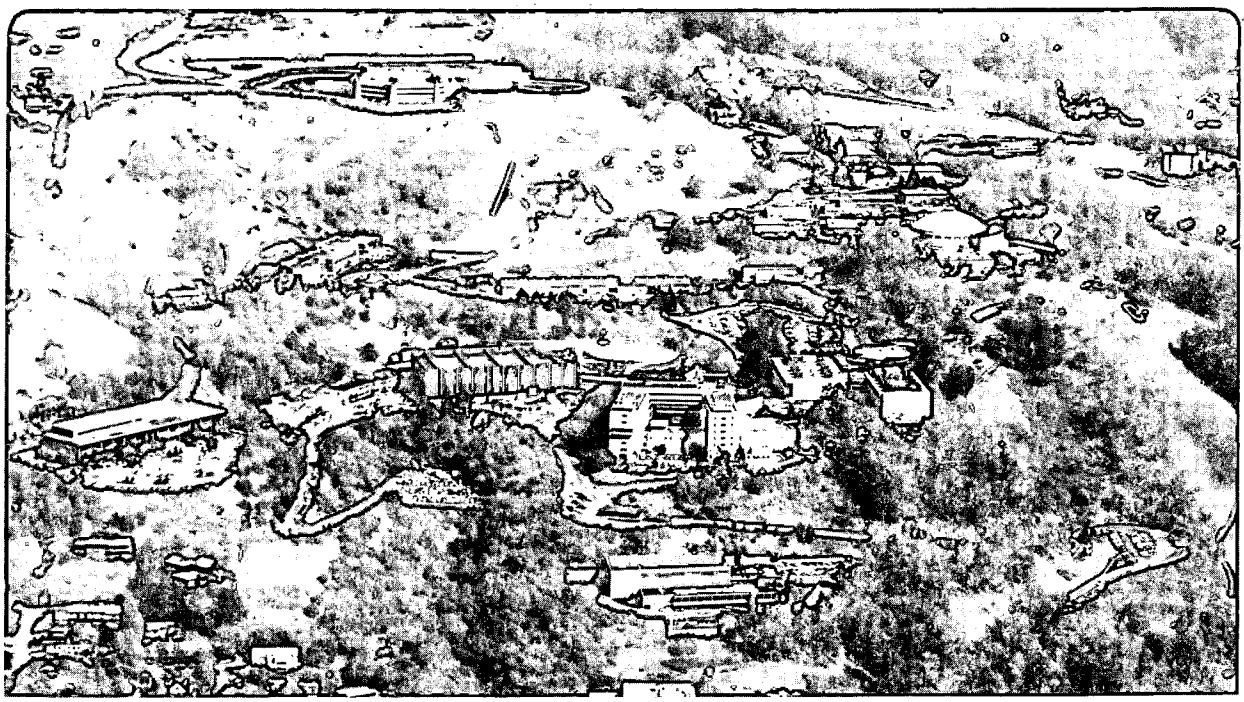

LBL-22840 c.2

Prepared for the U.S. Department of Energy under Contract DE-AC03-76SF00098

DISCLAIMER

This document was prepared as an account of work sponsored by the United States Government. While this document is believed to contain correct information, neither the United States Government nor any agency thereof, nor the Regents of the University of California, nor any of their employees, makes any warranty, express or implied, or assumes any legal responsibility for the accuracy, completeness, or usefulness of any information, apparatus, product, or process disclosed, or represents that its use would not infringe privately owned rights. Reference herein to any specific commercial product, process, or service by its trade name, trademark, manufacturer, or otherwise, does not necessarily constitute or imply its endorsement, recommendation, or favoring by the United States Government or any agency thereof, or the Regents of the University of California. The views and opinions of authors expressed herein do not necessarily state or reflect those of the United States Government or any agency thereof or the Regents of the University of California.

Description of Beam Position Monitor Signals with Harmonic Functions and their Taylor Series Expansions

Klaus Halbach
Lawrence Berkeley Laboratory
University of California
Berkeley, CA 94720

Abstract

Under most circumstances, appropriately processed signals from electric or magnetic beam sensing systems can be described by the real or imaginary part of the Taylor series expansion of an analytical function of a complex variable. This description can provide very good understanding of such signals and can be used to great advantage for the design of beam position monitor systems.

1) Introduction

Proper functioning and use of beam position monitors (BPM) are clearly of crucial importance for a number of accelerator systems, and the 1-2 GeV Synchrotron Radiation Source to be built at LBL is no exception. Trying to understand the consequences of tolerances on the beam location derived from signals obtained from the BPM that we intend to use on that machine, it developed that in addition to ideas developed for BPM analysis by other workers (see, for instance, References 1 through 3), methods that are regularly used in other fields (for instance, accelerator magnet technology) can be used very successfully in work on BPM. This paper represents an attempt to describe the application of these methods to the design and performance analysis of BPM. Trying to provide information to readers with a wide range of interests, both magnetostatic (MS) and electrostatic (ES) sensors will be discussed, but emphasis is on the latter type since that is the type of sensor we intend to use in our machine. Since it is the main purpose of this paper to explain the basic concepts, the details of the ES BPM system are explained only to the extent necessary to illuminate the

application of the general theory to a non-trivial system and to demonstrate some useful techniques for the design of BPM. In order not to get lost in careful formulations of all possible generalities, I restrict the detailed discussions in this first paper intentionally to the treatment of a fairly simple beam: all particles in the bunch have straight trajectories that are parallel to each other and parallel to the BPM symmetry axis, if such a symmetry axis exists. Signals from skew trajectories and other generalizations will be described in a follow-up paper.

2) Properties of BPM Signals

2.1) Motivation for Development of Stationary Signal Description

In many cases, BPM are used to diagnose highly relativistic beams of electrons. For the purposes of this discussion, I assume that I am dealing with a filamentary beam of electrons of uniform particle density in the longitudinal direction and of length L. Understanding the signals induced in the ES or EM sensors seems to be made very difficult by the radio frequency (RF) fields that are produced in the duct by the two ends of the bunch. One particular property of these fields is easy to understand if one represents the bunch of length L by linear superposition of a semi-infinite bunch of electrons, followed by a semi-infinite bunch of positrons that is axially displaced by L. Looking separately at the fields produced by the two semi-infinite bunches, the front end of the electron beam produces RF fields first. After the front end is well past the BPM section and the RF fields have decayed, what is left are the DC fields associated with the charge and current of the electron beam. It is clear that the positron beam produces <u>exactly</u> the same fields, except the polarity is reversed and the positron fields are delayed by L/c. If one integrates over time the charge induced on

the electrode of an ES sensor, or the flux induced in the pick-up coil of an MS sensor, and integrates until all fields in the BPM section have disappeared, one will obtain the difference in the "static" signals due to the displacement between the electron and positron beam. From this discussion it is clear that it is true, in general, that integration over the signals produced by any beam from the time before the fields "arrive" at the sensor until the bunch is well past the sensor and all fields have decayed, contain the "static" contributions and nothing else. By performing this integration one obviously gives up all information about the particle distribution in the axial direction. If that information is of great importance, one could get it preferably by a monitor that is optimized for this particular use or by using the BPM sensors with different processing of the primary signals. I assume here, and throughout this paper, that I need information about an individual bunch. If averaging over many bunches gives adequate information, the signal processing is obviously greatly simplified.

The signal seen by the MS system is the magnetic flux intercepted by the magnetic pick-up system. Since this flux itself has to be obtained by integration over the induced voltage, the MS system actually requires two integrations over time, while the ES system requires only one integration of the open circuit voltage over time. More details about implementation of these integrations will be given in Section 5.

2.2) Stationary Signal Properties Produced by a Filamentary Bunch

Equations (1) and (2) are the Maxwell equations that, together with the boundary conditions and the current density $\vec{j}(x, y, Z, t)$[4] and charge density $\rho(x, y, Z, t)$ of the bunch, determine the signals induced in the sensors.

$$\text{curl}\ \vec{H} = \vec{j} + \delta\vec{D}/\delta t \quad ; \quad \text{div}\ \vec{H} = 0 \tag{1}$$

$$\text{curl}\ \vec{D} = -\mu_0\varepsilon_0\delta\vec{H}/\delta t \quad ; \quad \text{div}\ \vec{D} = \rho \tag{2}$$

Since I am interested in the time-integrated flux or charge "seen" by the sensor, and since I am dealing with a linear system of differential equations, I can integrate Equations (1) and (2) over time <u>before</u> I solve them. Doing this, starting the integration before the fields arise and continuing until they have decayed, I get

$$\text{curl}\ \underline{\vec{H}} = \underline{\vec{j}} \quad ; \quad \text{div}\ \underline{\vec{H}} = 0 \quad , \tag{3}$$

$$\text{curl}\ \underline{\vec{D}} = 0 \quad ; \quad \text{div}\ \underline{\vec{D}} = \underline{\rho} \quad , \tag{4}$$

with the underlined symbols indicating quantities that have been integrated over time. This means in particular that $\underline{\vec{j}}$ and $\underline{\rho}$ are now non-zero over the whole trajectory of the bunch. The simplification due to the integration over time is very significant. One is dealing now with time independent equations, and to get the signal induced in the MS sensor, one has to solve only Equations (3), while the ES sensor signal is obtained from the solution of Equations (4). It is assumed throughout that on the surface of the duct, $\vec{D}$ is perpendicular to that surface, and $\vec{H}$ is parallel to it. Instead of solving Equations (3) and (4) directly for the time-integrals over the induced

flux/charge, I prefer to get that information by using reciprocity relationships, since that gives much more insight.

Dealing first with the magnetic pick up, one can show that the time integrated flux $\underline{\phi}$ induced by a filamentary $\vec{j}$ into a pick-up coil is given by the following volume integral:

$$\underline{\phi} = \int \vec{A}_3 \cdot \vec{j}\, dv/I_{oo} \quad . \tag{5.1}$$

In this equation, $\vec{A}_3$ is the vector potential produced if the current I_{oo} flows through the pick-up coil, and this "reciprocity" interpretation of the Green's function $\vec{A}_3$ is of great advantage both for understanding this equation as well as manipulating and using it. The generalization to non-filamentary $\vec{j}$ will be discussed in Section 2.3. Realizing that $\vec{j}$ integrated over time and (infinitesimal) cross section equals the charge Q in the bunch, and indicating by A_3 the Z-component of $\vec{A}_3$, the volume integral in Equation (5.1) yields

$$\underline{\phi} = Q \cdot \int A_3\, dZ/I_{oo} \quad . \tag{5.2}$$

For the ES sensor, one obtains a similar expression, with an equivalent reciprocity interpretation: If one puts the pick-up electrode on the scalar potential V_{oo}, with the rest of the duct surface being on zero potential, one can calculate the scalar potential V_3 everywhere inside the duct. The time integrated charge $\underline{q}$ on the electrode is then given by

$$\underline{q} = \int V_3 \cdot \underline{\rho}\, dv/V_{oo} \quad . \tag{6.1}$$

Realizing that ρ integrated over time and infinitesimal cross section equals the charge Q in the bunch divided by the velocity c with which the bunch moves, gives

$$\underline{q} = Q \cdot \int V_3 \, dZ/(cV_{oo}) \qquad (6.2)$$

That equations (5) and (6) are valid for a relativistic beam is a very remarkable fact: While V_3 (x, y, Z) describes indeed the signal "seen" by the sensor when a stationary or slowly moving electron is at location Z, this is not so for a relativistically moving electron or bunch: Because of the Lorentz contraction, the region of the duct that experiences first hand fields (as distinguished from excited RF oscillations) produced by a bunch is essentially not longer than the bunch itself. Considering the fact that these RF fields can be incredibly complex even for simple changes in duct crossection, Equations (5) and (6) can be viewed as rather remarkable conservation laws.

In Equations (5) and (6) the subscript 3 has been used to indicate explicitly that the potentials A_3 and V_3 are functions of the three space coordinates x, y, Z. Since one can assume without loss of generality that div $\vec{A}_3 = 0$, not only V_3 but also A_3 satisfies the three-dimensional (3D) Laplace equation. Since the integrals over Z go from a field-free region to a field-free region, these integrals are functions of the locations x, y of the bunch only and satisfy the two-dimensional (2D) Laplace equation and, as a consequence, $\underline{\phi}$ and $\underline{q}$ satisfy the 2D Laplace equation as well. Therefore, the study of the Z-integrals of A_3 and V_3 contain the whole information

required for $\underline{\phi}$ or $\underline{q}$, except for obvious amplitude multipliers like Q, Q/c. For that reason, below I deal with the integrated potentials, making the description of the needed information easier.

Turning again first to the MS case, I call the integrated vector potential A_3, normalized in any convenient way, A(x,y). Since it is invariably much easier to work with a harmonic function when one adds to it, with the appropriate factor +i or -i, the harmonically conjugate function, we do that here also. If V is the harmonically conjugate function to A, I define as the complex potential

$$F(z) = A + i V \quad ; \quad z = x + i y \quad . \tag{7.1}$$

Looking at the 2D field components B_x, B_y associated with A and also inspecting the expressions when B_x, B_y are derived from a 2D scalar potential, it turns out that V in Equation (7.1) is that scalar potential. Representing the 2D magnetic field vector B by the complex number $B = B_x + i B_y$, it also follows that

$$B^* = i \, dF/dz \quad . \tag{7.2}$$

Throughout this paper, the * indicates the complex conjugate of a complex quantity.

Proceeding similarly in the ES case, but making for that case the potential V the imaginary part of the complex potential, we get again Equation (7.1), and $E = E_x + i\ E_y$ is obtained from

$$E^* = i\ dF/dz \quad . \tag{7.3}$$

By describing the potentials of interest in this way, we need to study only one function F(z), but know that for the signal received by the MS sensor, we deal with the real part of F(z), Re F(z), and for the ES sensor signal, we have to look at the imaginary part of F(z), Im F(z).

Since the real/imaginary part of F(z) describes the signal received by a sensor, but can also be looked upon as the potential produced by the sensor if excited as described above in the formulation of the reciprocity principle, I use these two ways of interpretation interchangeably despite the fact that the actual excitation of the electrodes never takes place (except possibly for model measurements).

The determination of the location z of the beam is obviously simplified if the F(z) produced by a particular sensor is a nearly linear function of z, implying nearly homogenous fields in the region of interest. For that reason, I use the same mathematical technique that has proven to be so useful in similar circumstances, namely the analysis/design of 2D magnets: I expand F(z) in a Taylor series

$$F(z) = \sum_0 C_n\ z^n \quad . \tag{7.4}$$

2.3) Effects of Finite Transverse Beam Size

So far, it has been assumed that the beam has an infinitesimally small cross section. The generalization to a transverse charge/current distribution $p(x,y)$ (normalized so that $\int p(x,y)\, dxdy = 1$) is clear from the content of Section 2.2 and Figure 1: One has to replace $F(z)$ by

$$G(z) = \int F(z + w)\, p\,(u, v)\, du\, dv, \text{ with } w = u + i\, v \quad . \tag{8}$$

In this expression, z indicates the location of the center of an appropriately defined coordinate origin of the distribution function p. Using Equation (7.4) for F in Equation (8), one obtains after some manipulation

$$G(z) = \sum a_n\, z^n \tag{9.1}$$

$$a_n = \sum_{m=0} c_{n+m}\, p_m \binom{n+m}{m} \tag{9.2}$$

$$p_m = \int p(u,v)\, w^m\, du\, dv \tag{9.3}$$

The origin of the w-system is chosen such that $p_1 = 0$. In Section 2.4 the expression for the moments p_m of a number of distributions p are given. In all cases, it is assumed that the u-axis is parallel to the x-axis. If the p-distribution is rotated by the angle γ, each p_m has to be multiplied by $\exp(im\gamma)$.

Trivial as it may seem, I want to emphasize that Equations (9) apply also to "signals" that are weighted sums of signals from different sensors. As mentioned at the end of Section 3.2, this can lead to terms in $G(z)$ that are absent when one is dealing with a filamentary beam.

2.4) Moments p_m of Specific Distribution Functions p

Since I want to point out only a few somewhat surprising properties of distribution functions, I restrict myself to distribution functions that satisfy the condition $p(-u, -v) = p(u, v)$. Therefore, all $p_m = 0$ when m is odd. Conversely, whenever for odd $m \geq 3$, $p_m \neq 0$ are found, the distribution function is not invariant under rotation by π.

2.4.1) p_{2m} for p = const Within a Rectangle, p = 0 Outside Rectangle

With the notation of Figure 2, one obtains

$$p_{2m} = \frac{r_1^{2m}}{(m+1)(2m+1)} \cdot \frac{\sin\left((m+1)\alpha_1\right)}{\sin(\alpha_1)} \quad . \tag{10}$$

2.4.2) p_{2m} for p = const Within an Ellipse; p = 0 Outside Ellipse

With the notation of Figure 3, one obtains

$$p_{2m} = \frac{\left(x_0^2\,(1-\varepsilon^2)\right)^m}{m+1} \cdot \frac{1}{4^m}\binom{2m}{m} \sim \frac{\left(x_0^2\,(1-\varepsilon^2)\right)^m}{m+1} \cdot \frac{1}{\sqrt{\pi m}} \quad . \tag{11}$$

The second expression in Equation (11) is quite accurate for $m \geq 3$, and is given only to make (somewhat academic) comparisons easier.

2.4.3) p_{2m} for p = Bi-Gaussian Distribution Inside an Ellipse, p=0 Outside that Ellipse

In this case, the distribution function is given by

$$\begin{aligned} p &= \exp\left(-\left(u^2 + v^2/\varepsilon^2\right)/x_0^2\right) \quad \text{for } \left(u^2 + v^2/\varepsilon^2\right) < x_1^2 \\ p &= 0 \qquad\qquad\qquad\qquad\qquad \text{for } \left(u^2 + v^2/\varepsilon^2\right) > x_1^2 \end{aligned} \tag{12.1}$$

one obtains

$$p_{2m} = \left(x_0^2\,(1-\varepsilon^2)\right)^m \cdot \frac{1}{4^m}\binom{2m}{m} \cdot \left(m,\ (x_1/x_0)^2\right)! \Big/ \left(1 - e^{-(x_1/x_0)^2}\right) \tag{12.2}$$

$$p_{2m} \sim \left(x_0^2\,(1-\varepsilon^2)\right)^m \cdot \frac{\left(m,\ (x_1/x_0)^2\right)!}{\sqrt{\pi m}} \Big/ \left(1 - e^{-(x_1/x_0)^2}\right) \tag{12.3}$$

with

$$(m,\ x_1)! = \int_0^{x_1} e^{-x}\, x^m\, dx \tag{12.4}$$

2.4.4) Discussion of the Distribution Moments p_{2m}

A) Of the moments given above, only the ones for the rectangle provide information about both major dimensions of the beam cross section. For the other two, only one quantity, namely $x_0^2(1-\varepsilon^2)$, can be extracted.

B) $p_{2m} = 0$ in Equations (11) and (12) for $\varepsilon = 1$. These are special cases of the general theorem, following directly from Equation (9.3), that for <u>any</u> axisymmetric distribution, all $p_m = 0$ for $m > 0$. One should notice that both this statement, and the ones made above (A), are independent of the method one chooses to describe the sensor signals.

C) Letting $(x_1/x_0)^2$ in Equations (12) be reasonably large, it is interesting to note that until m is of order $(x_1/x_0)^2$, p_{2m} grows with m like $\sqrt{m}\,(m-1)!$ for the bi-Gaussian distribution, while it goes down like $1/\,m\,(m+1)$ for the elliptical hard edge distribution, showing the great

importance of the tails of the bi-Gaussian distribution. When m gets large enough, the hard edge cut off of the bi-Gaussian makes itself felt and ultimately its p_{2m} behaves similarly to p_{2m} for the elliptical hard edge distribution. While all of this is somewhat academic, considering the difficulty to measure p_{2m} for large m, it still gives some insight into what might happen under extreme circumstances, and it allows one to estimate the value of higher order p_{2m} if only p_2, or p_2 and p_4, have been measured.

3) Some Guidelines for the Design of Ducts and Sensors

The main information one wants to obtain from a BPM are the coordinates x,y of the beam centroid. In addition, one usually does not know the charge Q in the bunch, so that one needs at least three sensors to determine x, y, Q. While these three sensors are sufficient in principle to get the desired information when the beam size effects are small enough or known, one usually employs four sensors. This provides some redundancy, and I assume below that at least four sensors are used.

3.1) Consequences of Sensor Geometry Errors

Figure 4 shows schematically a pick-up electrode for an ES sensor system. The solidly drawn line shows the electrode as it is supposed to be located. The dashed line shows the actual surface of the electrode due to an installation error, and I want to know how that affects the performance of the sensor. To get that information, I use the reciprocity principle and determine the errors in the potentials produced by the electrode when it is put on a potential. In order to get an understanding of the changes in potentials in the duct, I imagine the surface charges on the electrode to be separated from the metal and remove the metal down to the dashed line. Since the charges were kept in place, no change in potentials occurred. As the last step, I remove the charges that were "left behind" (or put charges of opposite-

polarity there), and the resulting changes in potential are exactly the potential changes due to the movement of the electrode. It is clear that there will be, as a consequence, also mirror charges on the electrode surface, so that the net effect is essentially the same as an electric dipole located on the surface of the electrode, and one can show that this is essentially equivalent to a change in sensor sensitivity. Since the associated dipole moment is proportional to the charge on the moved surface, it is clearly advantageous to not make that charge larger than necessary. Figure 5 shows the charge on the surface of the circular electrode as a function of the ratio of the dimensions r_2 and r_1 shown in Figure 4. It is clear from that graph that one should not make r_2/r_1 much smaller than 1.1, and that conditions do not improve significantly if one makes r_2/r_1 substantially larger. One can draw from this consideration also two other conclusions: A) One may reduce the sensitivity to the "flushness" of the electrode with the duct wall significantly if one breaks up the electrode into a number of rods so that most electric field lines end on surfaces that are perpendicular to the wall surface; and B) Sensitivity to deformation of the wall is greatest where, upon excitation of a sensor, the wall has the largest electric field.

The same logic can be applied to a magnetic pick-up strip. Figure 6 shows schematically a cross section of a duct and a magnetic pick-up conductor. The conductor has no sharp edges to avoid large magnetic fields on the surface. It is interesting to note that most of the region of the largest surface field is close to the wall and, in a sense, shielded from "view" of the beam.

3.2) General Symmetry Properties of BPM Systems

Symmetry properties of BPM systems have the consequence that simple relations exist between the expansion coefficients associated with the individual sensors. Because of these relations, certain combinations of signals (for instance the sum of all signals, needed to find the charge in the bunch) are described by Taylor series expansions with some expansion coefficients being exactly zero and/or coefficients having distinct and predictable phase angles. Two kinds of symmetry are possible: 1) invariance of the geometry of the system to rotation by an angle $2\pi/M$ (M usually equals an even integer; the lowest nontrivial order with M=2 in the case of the system shown in Figure 7), and 2) mirror symmetry with respect to one or more axes (namely the x-axis and y-axis of the system shown in Figure 7). Systems often have both symmetry properties simultaneously, but any one of the two conditions may be satisfied alone, i.e. without the other being valid.

In case of rotational symmetry, it is easy to show that if C_n are the expansion coefficients associated with the reference sensor, then the coefficients $C_n(m)$ associated with a sensor at the location rotated by $m \cdot 2\pi/M$ relative to the reference sensor are given by:

$$C_n(m) = C_n \exp(-inm\, 2\pi/M) \quad . \tag{13}$$

As a consequence, the sum of all sensor signals is then given by the real or imaginary part of

$$F(z) = M \cdot \sum_{n=0} C_{Mn}\, z^{Mn} \quad . \tag{14.1}$$

If M is even and one takes the sum with alternating signs, one gets

$$F(z) = M \cdot \sum_{n=0} C_{Mn+M/2} \cdot z^{Mn+M/2} \tag{14.2}$$

Equations (23.1) and (23.2) in Section 4.3.1 are a direct consequence of Equation (13). Equation (23.3) describes the relationship between the expansion coefficients of an ES sensor system that has mirror symmetry with respect to the x-axis.

The fact that the complex potentials given by Equations (14) have a much smaller number of terms than normal is, as such, <u>not</u> a strong motivation for wanting a high degree of rotational symmetry: Having this mathematical description of BPM signals, it is fairly easy to obtain values for all relevant coefficients C_n. Reducing the number of relevant coefficients therefore reduces under most circumstances only the computational effort needed to obtain the values for the desired quantities (such as x, y, Q). That reduction of computational effort is not important unless one has to obtain the final answers very fast in order to perform tasks like applying real time corrections. However it is clear that the absence of certain harmonics or the exact phase of the coefficients is disturbed when one is dealing with a non-filamentary beam that does not have the same symmetry characteristics as the sensor system, thus leading to easily identifiable signal properties from which one can draw conclusions about beam characteristics. In fact, this is often the only reasonable way to get specific pieces of information.

While it is therefore true that in many cases it is advantageous to have a sensor system with the highest possible degree of symmetry, one has to be careful <u>not</u> to accept this principle without a very careful examination of all details of a specific system. In Section 4.3.3 a detailed set of circumstances is discussed where one needs to deliberately <u>destroy</u> symmetry properties in order to be able to determine x, y.

The reason for this cautionary note is the fact that BPM have to meet a bewildering variety of conditions and requirements, as the following incomplete list of double choices indicates:

- Distribution function moments p_m have (no) effect on the determination of x, y, Q.
- Q is (not) known from other diagnostic devices.
- The phases of the p_m, i.e. the orientation of the density distribution, are (not) known.
- $p_m=0$ ($\neq 0$) for odd m.
- Knowledge of p_m is (not) required.
- Other overall system requirements (e.g. vacuum system) do (not) impose severe restrictions on duct geometry.
- Moving the beam from one known z to another is (not) permitted.
- (No) more than 4 sensors can be placed in duct.
- 2D geometry, as defined in Section (4.1), can (not) be implemented.
- Averaging over many bunches is (not) adequate.

To complicate matters a little more, the set of restrictions and requirements will be different during primary machine use than during machine improvement time.

3.3) The Importance of Correct Gains

The sensor location error discussed in Section 3.1 is equivalent to an overall gain error in that channel. To show how important correct overall gains are, I take the difference between two signals coming from two sensors whose angular positions are π apart in a four-fold symmetry system, and I take only the dominant, namely linear, term. I get

$$\Delta G = 2\, a_1\, z \quad . \tag{16}$$

The consequence of having one gain being off by the relative error ε is equivalent to adding to the right side of Equation (16) εa_0, which cannot be distinguished from a small beam displacement of order $\varepsilon\, a_0/(2a_1)$.

3.4) Preferred Location of ES Sensors

Systems that do not have a high order of symmetry have to satisfy, aside from orientation, some sensor location requirements to function properly. Figure 7 shows a cross section of a duct with a geometry that is invariant to rotation by the angle π, and has two symmetry planes. Shown is also the location of ES sensor 1, and the other three sensors that I always assume to be located symmetrically as shown. It is qualitatively clear that if sensor 1 is placed close to the right corner of the duct (and the other sensors placed accordingly), one will get very poor information about the y coordinate of the beam center. Similarly, if sensor 1 is placed close to the top, the x coordinate of the beam center will be poorly known. To give a good understanding of these matters, I want to formulate these facts quantitatively for this simple case.

If I take the difference S_1 between the signals from sensors 1 and 3, I clearly get no signal if the beam center is at $x = y = 0$. Taking only the dominant linear term into account, I get

$$S_1 = a \cdot \vec{\underset{\sim}{E}} \cdot \vec{r} \tag{17}$$

when the beam center is at location (x, y), if I call the Z-integral over the "reciprocity" field $\vec{\underset{\sim}{E}}$, and if I absorb all other factors in a. If $\underset{\sim}{E}$ has the magnitude E_0, and forms the angle γ with the x-axis, I get

$$S_1 = a\, E_0\, (x \cos \gamma + y \sin \gamma) \tag{18.1}$$

Because of symmetry, I get from sensors 4 and 2

$$S_4 = a\, E_0\, (x \cos \gamma - y \sin \gamma) \tag{18.2}$$

I assume now, for simplicity's sake, that I know the charge Q in the bunch, either from summing all four signals, or some other source. Consequently, the constant a is known in addition to S, E_0 and γ, and I get for x and y

$$x = \frac{S_1 + S_4}{2a\, E_0 \cos \gamma} \quad ; \quad y = \frac{S_1 - S_4}{2a\, E_0 \sin \gamma} \tag{19}$$

Because in Equation (19) the sums and differences of measured quantities occur that are "afflicted" with statistically independent measurement errors ΔS_1, ΔS_4, the errors of the so determined values of x and y are proportional to $1/\cos\gamma$ and $1/\sin\gamma$. If the required accuracy of the x and y determination is about equal, γ should therefore not deviate significantly from $\pi/4$.

4) 2D Systems

4.1) Advantages of 2D System Geometry

Everything discussed in the above sections is valid for 3D geometry, including the statements (and consequences) that the integrals in the axial direction of the 3D potentials satisfy the 2D Laplace equation. Unfortunately, calculating these 3D potentials and/or these integrals is not easy in 3D geometry. If, however, one is dealing with 2D geometry in the sensor region and its immediate vicinity, these integrals can be obtained directly by solving the Laplace equation in 2D geometry either with conformal mapping techniques (as shown below) or 2D computer codes such as POISSON. By "immediate vicinity" is meant that the duct cross section should not change (i.e., should be 2D) over a total axial length that is not less than about three times the characteristic transverse dimension. The reason for this is the fact that "reciprocity" potentials produced by excited sensors decay in the axial direction by at least about a factor 100 every time one advances axially by a distance equal to the transverse dimension.

The simplifications associated with 2D geometry are so enormous both for thinking about the sensors as well as performing computations that it is worthwhile to go to great lengths in order to achieve 2D conditions with reasonable validity. While 2D conditions require only that non-protruding pick-up electrodes are flush with the duct surface, conditions are more

difficult for magnetic pick-up loops or protruding pick-up electrodes. For instance, since one usually prefers not to have pick-up loops protruding into the essential duct volume, one often increases the duct cross section to accommodate the sensor. In order to achieve 2D conditions, one should extend this enlarged cross section over a sufficient axial length. If the pick-up conductor has such a cross section and orientation to modify significantly the field produced by the beam to be used, one should have identical dummy conductors adjacent to both axial ends of the sensor, and they should extend over the whole length of the 2D cross section.

4.2) Relationship Between 2D Potentials and Line Integrals over Potentials Produced by a Short Sensor

In the following discussion I keep x, y fixed, but the result holds for every value of x, y, with appropriate values for v_0 derived from the complex potential for every x, y.

In 2D geometry, let the value of the potential at location Z, dv(Z), produced by a sensor of length dZ_0 at location Z_0, be given by

$$dv(Z) = f(Z - Z_0)\, dZ_0 \quad .$$

I then get for an infinitely long sensor

$$v_0 = \int_{-\infty}^{\infty} f(Z - Z_0)\, dZ_0 \tag{20}$$

and this is, of course, the potential v_0 obtained from a 2D calculation. For a sensor extended from Z_1, to Z_2, I get

$$v(Z) = \int_{Z_1}^{Z_2} f(Z - Z_0)\, dZ_0 \quad . \tag{21}$$

The value of $\underline{v} = \int_{-\infty}^{\infty} v(Z)\, dZ$ is obtained from Equation (21), and one gets after exchanging the order of integration:

$$\underline{v} = \int_{Z_1}^{Z_2} \int_{-\infty}^{\infty} f(Z - Z_0)\, dZ\, dZ_0$$

With Equation (20), this becomes

$$\underline{v} = \int_{Z_1}^{Z_2} v_0\, dZ_0 = v_0(Z_2 - Z_1) \tag{22}$$

i.e., the line integral over the potential equals the 2D potential produced by an infinitely long sensor, multiplied by the actual length of the sensor. The effects of sensors like round electrodes mounted flush in the wall of a duct can be obtained by linear superposition of the effects caused by electrodes of appropriate lengths at appropriate locations in the 2D cross section of the duct.

4.3) Design and Properties of a Specific ES System

Figure 7 shows schematically a system that is somewhat simpler but similar to the one we may use on the LBL 1-2 GeV Synchrotron Radiation Source, and I

want to use that system as an example to demonstrate the application of the formulae and procedures developed here.

The duct geometry shown in Figure 7 is not freely chosen but imposed by vacuum system requirements. To design and analyze that system without getting lost in basically uninteresting details, I calculate first the expansion coefficients for the complex potentials produced by excitation of very short electrodes. This will demonstrate both some conventional but useful techniques and provide the basis to discuss some properties and options of this type of system.

4.3.1) Relationship Between Expansion Coefficients Describing the Complex Potentials Associated with Different ES Sensors

Since the geometry is invariant to rotation by the angle π, the expansion coefficients $C_n(3)$ associated with sensor 3 are related to the expansion coefficients $C_n = C_n(1)$ associated with the reference sensor 1 and are given by

$$C_n(3) = (-1)^n C_n \quad . \tag{23.1}$$

For the same reason,

$$C_n(4) = (-1)^n C_n(2) \quad . \tag{23.2}$$

Realizing that the scalar potential $V_4(x, -y)$ produced by sensor 4 at location $(x, -y)$ is the same as the scalar potential $V_1(x, y)$ produced by sensor 1 at location (x, y) leads to

$$C_n(4) = -C_n^* \quad , \tag{23.3}$$

giving with Equation (23.2):

$$C_n(2) = -(-1)^n C_n^* \tag{23.4}$$

For MS sensors, the right hand sides of Equations (23.3), (23.4) have to be multiplied by -1.

4.3.2) Calculation of Expansion Coefficients C_n for Sensor 1

In order to calculate F(z) and the expansion coefficients C_n, I map the interior of the duct in Figure 7 onto a circular disk with radius 1 in an auxiliary w-plane, shown in Figure 8 with the location of the maps of points 1, 1', 2', 3', 4'. This transformation is governed by the Schwartz-Christoffel formula

$$dz/dw = (1 + w^2)^{-n_1} \cdot (1 - w^2)^{-n_2} \; ; \quad n_1 = \beta/\pi; \; n_2 = \alpha/\pi; \; n_1 + n_2 = 1 \tag{24}$$

A freely choosable multiplicative constant on the right side of Equation (24) has been set equal one, to get dz/dw = 1 for w = 0 ←—→ z = 0. This means that all "real" dimensional transverse lengths have to be multiplied by a constant k to convert to the dimensionless lengths of this theory, and

k = (dimensionless distance in the geometry mapped with Equation (24) onto the circular disk)/(dimensioned length of same distance in real geometry). (25)

A convenient length for this conversion is the dimensionless distance D_1, which can be obtained by integrating Equation (24) along the imaginary w-axis. After introduction of a new variable to remove the singularity of the integrand at w = i, one obtains

$$D_1 = \frac{1}{n_2} \cdot \int_0^1 \frac{dv}{1+w} \left(\frac{1+w}{1+w^2}\right)^{n_2} \quad ; \quad w = 1 - v^{1/n_2} \quad . \tag{26}$$

The general solution of the Dirichlet problem in a circular disk is given by

$$F(w) = \frac{i}{\pi} \cdot \left(\frac{1}{2} \int_0^{2\pi} V(\Psi)\, d\Psi + w \int_0^{2\pi} \frac{V(\Psi)}{e^{\Psi} - w}\, d\Psi \right) \quad . \tag{27}$$

For simplicity, I assume a sensor of infinitesimal width $\Delta\Psi_1$ at Ψ_1 where $V = 1$, V being zero elsewhere on the duct surface. This gives for the multipole expansion in the w plane

$$F(w) = \frac{i\Delta\Psi_1}{\pi} \left(\frac{1}{2} + \sum_1 w^n e^{-in\Psi_1} \right) \quad . \tag{28}$$

A formula similarly useful for MS sensors is the expression for the complex potential within a circular disk with radius one that has a filamentary current I_{oo} at location W_o and has $A = 0$ on its boundary:

$$F(w) = \frac{-I_{oo}}{2\pi} \cdot \ln \frac{w_o - w}{1 - w\, w_o^*} \quad .$$

Equation (24) contains all needed information to expand w in a Taylor series in z, to be then used in Equation (28) to get the expansion coefficients C_n. For more complicated systems than this one, all of this

can easily be executed (with the help of a Taylor series coefficient manipulation subroutine package) with a computer. In the case of the simple mapping function involved here, an explicit expression for $C_0 - C_6$ is easily derived and these coefficients are given by Equations (30) with the following abbreviations:

$$g_1 = \Delta\Psi_1/\pi \;;\; d_3 = (2n_1 - 1)/3 \;;\; d_5 = 2.1\, d_3^{\,2} - 0.1 \tag{29}$$

$$C_0 = i\, g_1/2 \tag{30.0}$$

$$C_1 = i\, g_1 \exp(-i\, \Psi_1) \tag{30.1}$$

$$C_2 = i\, g_1 \exp(-2i\, \Psi_1) \tag{30.2}$$

$$C_3 = i\, g_1 (d_3 \exp(-i\, \Psi_1) + \exp(-3i\, \Psi_1)) \tag{30.3}$$

$$C_4 = i\, g_1 (2\, d_3 \exp(-2i\, \Psi_1) + \exp(-4i\, \Psi_1)) \tag{30.4}$$

$$C_5 = i\, g_1 (d_5 \exp(-i\, \Psi_1) + 3\, d_3 \exp(-3i\, \Psi_1) + \exp(-5i\, \Psi_1)) \tag{30.5}$$

$$C_6 = i\, g_1 ((2\, d_5 + d_3^{\,2}) \exp(-2i\, \Psi_1) + 4\, d_3 \exp(-4i\, \Psi_1) + \exp(-6i\, \Psi_1)) \tag{30.6}$$

Except for the scaling factor g_1, common to all coefficients C_n, the duct geometry enters through the parameters d_3 and d_5 in Equations (30). It is interesting to note that d_3 enters into these equations for the first

time in Equation (30.3), and d_5 enters for the first time in Equation (30.5). This is a general behavior of these equations when the duct geometry is invariant to rotation by the angle π. More details of this nature will be described in a forthcoming paper.

The relationship between the length $\Delta\Psi_1$ of the sensor in w geometry and the length $|\Delta z|$ in z - geometry follows directly from Equation (24):

$$\Delta = |\Delta z| \cdot 2 \sin^{n_2}\Psi_1 \quad \cos^{n_1}\Psi_1 \tag{31}$$

It should be noted that the absolute values of all C_n shown above are of the same order, namely of order g_1. While this changes somewhat for higher order coefficients when the width of the sensors becomes large (the C_n become smaller), it still makes the assessment of the relative size of contributions from different sources to F easy. The magnitudes of contributions are determined (when one ignores phases) by powers of normalized distance from z = 0 and the p_m, which are controlled, crudely speaking, by asymmetry and beam size.

Inspecting Equation (30.1), it is clear that the angle Ψ_1 should equal approximately $\pi/4$ to satisfy the requirements stated in Section 3.4. It is a simple matter of integrating dz/dw to get the corresponding location of the sensor in the z-plane.

4.3.3) Use and Discussion of a Specific ES Sensor System

When one has measured the time integrated charges at the four sensors shown in Figure 7, one has to calculate from these four values the location of the beam center (x, y), the charge in the beam (Q), and p_2 if it is large enough. Instead of looking directly at the complex potentials representing the four different sensors, it is advantageous to inspect the sums and differences as shown symbolically in Equations (32). These expressions represent the same total information as the complex potentials for the individual sensors, but show it in a form that is much easier to understand and use.

If sensor 1 is characterized by the coefficients C_n with real and imaginary parts R_n, J_n;

$$C_n = R_n + iJ_n \quad , \tag{32.0}$$

one gets for the sums and differences symbolically indicated to the left of the equations

$$\begin{matrix} - & + \\ - & + \end{matrix} \; F_1(z) = 4 \sum_{n=0} iJ_{2n+1} \, z^{2n+1} \quad , \tag{32.1}$$

$$\begin{matrix} + & + \\ - & - \end{matrix} \; F_3(z) = 4 \sum_{n=0} R_{2n+1} \, z^{2n+1} \quad , \tag{32.3}$$

$$\begin{matrix} - & + \\ + & - \end{matrix} \; F_2(z) = 4 \sum_{n=1} R_{2n} \, z^{2n} \quad , \tag{32.2}$$

$$\overset{+\,+}{+\,+}\ F_4(z) = 4 \sum_{n=0} iJ_{2n}\, z^{2n} \quad . \tag{32.4}$$

The equivalent formulae for a MS system are obtained from Equations (32.1) - (32.4) by replacing everywhere R_m by iJ_m, and iJ_m by R_m. To obtain the functions G(z) that describe finite size beams, one has to calculate from the coefficients appearing in Equations (32) the coefficients a_m with Equation (9), and the first few of these are given explicitly in Equations (33).

$$a_o = C_o + C_2\, p_2 + C_3\, p_3 + C_4\, p_4 + \ldots \tag{33.0}$$

$$a_1 = C_1 + C_3\, p_2 \cdot 3 + C_4\, p_3 \cdot 4 + C_5\, p_4 \cdot 5 + \ldots \tag{33.1}$$

$$a_2 = C_2 + C_4\, p_2 \cdot 6 + C_5\, p_3 \cdot 10 + C_6\, p_4 \cdot 15 + \ldots \tag{33.2}$$

$$a_3 = C_3 + C_5\, p_2 \cdot 10 + C_6\, p_3 \cdot 20 + C_7\, p_4 \cdot 35 + \ldots \tag{33.3}$$

To obtain the actual signal amplitudes, one has to multiply the imaginary part of G with the charge in the bunch and a number of known factors (gains, 1/c, length of sensors, etc.). However, since these simple steps are needed only to get the bunch charge from Im G_4, I do not carry them out in detail, but work directly with the F and G functions.

With the length normalization used here, all $|C_n|$ are of order one, and the $|p_m|$ are of order $(x_0\sqrt{1-\varepsilon^2}/\text{duct dimension})^m$. With duct dimensions of the order 10 mm, and fully damped beam dimensions of the order of 10 μm, the p_m can be ignored for that case, and I want to discuss that simple case first.

To obtain x and y, one simply looks at the ratio of signal $S_1/S_4 = \text{Im } F_1/\text{Im } F_4$, and similarly $S_3/S_4 = \text{Im } F_3/\text{Im } F_4$. Since the ratios of the known signals are ratios of known functions, it is an easy matter to solve these two equations for the two unknowns x, y. While the non-linear term coming from J_2 in Equation (32.4) can be made to vanish by choosing $\Psi_1 = \pi/4$ in Equation (30.2), doing that is not a matter of high priority for two reasons: 1) There are also non-linear terms coming from Im F_1, Im F_3 which are practically unavoidable. 2) Non-linear terms are not of great concern since their structure (i.e. harmonic polynomials) and coefficients are well understood and known, resulting therefore only in a slight computational inconvenience without incurring errors.

Solving for x and y is easily done by applying the 2D Newton's method. In most cases it is probably even sufficient to proceed as follows: Take y as a factor out of Im F_3 and solve trivially for that y, i.e. express y in terms of S_3/S_4 and terms that are non-linear in x, y. Solve similarly for x. Solve then for (x, y) iteratively by computing new values (x, y) from old values in the non-linear terms, starting there with x=y=0. Unless $|z|$ is quite large, this process will converge very rapidly. One should notice that $S_2 \sim \text{Im } F_2$ has not been used for this procedure. One can use this signal to check for errors and self consistency. Should one of the sensors be disabled, one clearly has still enough information to determine x, y.

The case of non-ignorable p_m is much more complex. These circumstances may arise during injection into a ring, and it is therefore more than an interesting hypothetical case.

If $p_3 \neq 0$, Equations (32) and (33) show that terms appear in G_1, G_3, G_2, G_4 that are normally absent. In particular, depending on the phase of p_3, constant (i.e. z-independent) terms appear in G_1 and G_3 that can be misinterpreted as a displacement of the beam. To determine the, generally complex, value of p_3 one needs to measure the sensor signals when the beam is at several known values of z.

To demonstrate another specific and very important point, I discuss next the case where only p_2 is noticeable, p_3 being absent because of symmetry, and higher order moments being much too small to be seen. Furthermore, p_2 is real as it is in the "normal" case where the mirror symmetry axes of the beam and the BPM system are the same, namely the x and y axes. Under these circumstances, it can occur that an accurate determination of the beam center is impossible despite the fact that one has four signals to determine the four unknowns x, y, Q, p_2. This is most easily demonstrated by assuming that y=0. Equations (32) and (33) show that in that case Im G_2 = Im G_3 = 0, leaving only Im G_1 and Im G_4 to determine x, Q and p_2. Equations (32.1) and (33.1) show that the term linear in z in G_1 has the coefficient $a_1 = 4 \cdot i(J_1 + 3J_3\, p_2)$, i.e. p_2 has a significant effect on Im G_1. One can show furthermore that in Im G_4, the constant term is modified in a different manner by p_2 than the linear term in G_1, thus making it impossible to determine any of the wanted quantities accurately. The case x=0 leads to the same conclusion.

If one is restricted to four sensors this problem can be avoided only if the mirror symmetry axes of the beam and BPM system form a known angle δ between 0 and $\pi/2$, p_2 thus given by $|p_2| \exp(-2i\delta)$. As is easily seen from Equations (32.2) and (33.0), G_2 then has a term $a_0 = 4 R_2 \cdot p_2$ with a non-vanishing imaginary part, allowing now solving for all four unknowns. In the case of the storage ring that serves as the example here it is impossible to rotate the whole duct, leaving as the only option the movement of sensors 1 and 4 in opposite directions on their respective duct walls, with sensors two and three moving correspondingly to still maintain invariance of the system geometry to rotation by π. In reality, vacuum system requirements require an opening of the duct on one side, so that the need to determine (x, y) in the presence of a noticeable p_2 requires abandonment of the only symmetry that the original system possessed.

If it is possible to have BPM with six (or more) sensors, the problems arising from noticeable p_2 values can be solved without destroying symmetry properties, clearly a much more desirable solution. Without going into details, the reader is also reminded that during machine improvement period of such a ring, a lot of valuable information can be gathered if one measures sensor signals with the beam at known locations. A particularly useful procedure would be observation of the beam when it is being moved to and measured at equidistant locations on the circumference of as large a circle as possible. This allows determination of all complex coefficients a_n in G that contribute to the signals, from which one can then determine the p_m up to the highest contributing order.

5) Integrators

Having integrators with exactly the right properties is very important. The reasons are simple: If the analog signal processing is done incorrectly, the RF field can contribute to the system output in a way to falsify the results, the results will be erroneous if the bunch length changes, etc.

Since neither the ES pick-up electrodes nor the MS pick-up loop look into an infinitely large external impedance, the following signal processing system has to accommodate that and will therefore be slightly different from a single or double integrator. However, to understand what such a system should do, one has to understand what the overall signal processing system has to look like, including the impedances that the sensors "see".

It is convenient to use the response function H(t) to a δ- function at $t = 0^-$ to describe the overall system properties. It is clear that the ideal response functions for the single and double integrator shown in Figure 9 are not realizable. On the other hand, one really needs <u>very good</u> integrators if one wants to make good beam position measurements. The more difficult of the two integrators is the double integrator. It will be shown that a nearly perfect double integrator may have a response function H(t) that is very different from the one shown in Figure 9. In order to arrive at that conclusion, one has to discuss first the single integrator in considerable detail.

5.1) The Single Integrator

5.1.1) General Properties of the Single Integrator

I describe the input signal by $S_0(t)$. It consists of the "static" part shown in Figure 10, preceded, superimposed, and followed by the RF contamination that integrates out to zero. $t = 0$ is set such that $S_0(t) = 0$ for $t < 0$, and T_1 is the time beyond which $S_0(t) = 0$. One can express the purpose of the integrator in the following way: One wants to determine

$$M_n = \int_0^{T_1} S_0(t)\, t^n\, dt \tag{34}$$

for $n = 0$ with as little "contamination" by M_n with $n > 0$. In order to understand all aspects and properties of the integrator that are important for the design, I look at the integrator from several perspectives, and the starting point is the following:

The output signal $S_1(t)$ is given by

$$S_1(t) = \int_0^{T_1} S_0(\tau)\, H(t-\tau)\, d\tau \tag{35}$$

Expanding H (t -) about t, one gets

$$S_1(t) = \sum_{n=0} H^{(n)}(t)\, (-1)^n\, M_n/n! \tag{36}$$

The basic philosophy for the design of a good integrator follows from Equations (35) and (36): If the M_n are sufficiently small for $n > 0$, $S_1(t) \sim M_0\, H(t)$, and by measuring the maximum value of $S_1(t)$, occurring at the time when $H(t)$ has a maximum, I have determined M_0 very

accurately, no matter what H(t) looks like before or after the time when H_{max} has been reached. If, on the other hand, the M_n contribute significantly to S_1, at the time S_1 reaches it maximum value, I can change that by "designing" H(t) such that at the time of $\dot{H} = 0$, $\ddot{H}$ and $\dddot{H}$ are very small or zero. In other words, I make H(t) in the vicinity of $\dot{H} = 0$ very flat, and a specific model function that satisfies these conditions will be discussed below. How this works is also clear from Equation (35): If H(t) were completely flat for a time T_1, I could measure M_0 exactly. Deviations from this flatness over that length of time simply have to be sufficiently small to not cause difficulties.

To understand the importance of the time scale of the response function H, I now use

$$H(t) = H_1\ (t/T_0) \tag{37}$$

and try to find out how $S_{1\ max}$ depends on the time scale T_0 of the response function. Using Equation (37) in Equation (35), with $\varepsilon = 1/T_0$, and the dimensionless time $u = \varepsilon t$, I get

$$S_1(t) = \int_0^{T_1} S_0(\tau)\ H_1\ (u - \varepsilon\tau)\ d\tau \quad . \tag{38}$$

To evaluate how $S_{1\ max}$ depends on ε, I expand the (normalized) time u at which $\dot{S}_1 = 0$ in a power series in ε:

$$u = u_0 + \varepsilon b_1 + \varepsilon^2 b_2 + \ldots\ , \text{ with } H_1'\ (u_0) = 0 \quad . \tag{39}$$

Using that in

$$\dot{S}_1(t) = \int_0^{T_1} S_0(\tau)\ H_1'\ (u_0 + \varepsilon\ (b_1 - \tau\ ) + \varepsilon^2\ a_2 + \ldots)\ \ d\tau/T_0 = 0 \tag{40}$$

yields immediately

$$b_1 = M_1/M_0 \quad , \tag{41}$$

and using that in Equation (38) yields

$$S_{1\ max} = \int_0^{T_1} S_0(\tau)\ H_1\ (u_0 + \varepsilon\ (b_1 - \tau\ ) +)\ d\tau \tag{42}$$

Expanding H_1 in ε and observing again that $H_1'(u_0) = 0$ gives, after collecting terms:

$$S_{1\ max} = H_1\ (u_0)\ .\ M_0 + \varepsilon^2\ .\ H_1''\ (u_0)\ (M_2 - M_1{}^2/M_0) + \ .\ .\ .\ . \tag{43}$$

The important consequence of this equation is that if one lengthens the time scale of H(t), one reduces at least quadratically the contribution of unwanted higher moments of S_0 to $S_{1\ max}$.

If one takes this consideration one step further and makes not only $H_1'(u_0) = 0$, but also $H''(u_0) = 0$ and $H_1'''(u_0) = 0$ ($H_1'''(u_0) = 0$ is necessary if $H_1(u_0)$ is to have a maximum when $H'(u_0) = H''(u_0) = 0$), the dominant term containing higher moments of S_0 than M_0 is proportional to ε^4. This indicates that making the first three derivatives of H simultaneously zero and increasing the time scale for H(t) are very advantageous procedures.

While simultaneously making the first three derivatives of H zero is a good starting point for a good design of H(t), one can show that giving $\ddot{H}$ a slightly positive value (where $\dot{H} = 0$, $\dddot{H} = 0$) increases the length of time during which H(t) is within a given small fraction of its peak value by about a factor two. While it is clearly advantageous to implement this in a real system, I will not discuss this for either the single or double integrator in

more detail since the implementation is clearly not difficult if one can design a system that satisfies the more basic condition that the first three derivatives of H are zero at the same time.

In this whole section I have always assumed that M_0 is obtained from S_{1max}. In practice one may not want to do this because of the presence of the RF signals. Since one usually knows when a bunch comes, or since one can determine when $S_1(t)$ starts to rise, one might prefer to read $S_1(t)$ at a given appropriate time.

5.1.2) $H_1(u)$ for a Specific Single Integrator

In order to find out whether or not it is possible to design a "reasonable" function that satisfies $H_1'(u_0) = H_1''(u_0) = H_1'''(u_0) = 0$, I have tried to design such a function. In this context, reasonable means a function that does not violate conditions that all analog systems must satisfy, like high frequency behavior. In addition, it should be easy to determine essential parameters with analytical methods. One such function is

$$H_1(u) = ue^{-u} + a\alpha e^{-\alpha u} \quad . \tag{44.1}$$

The Laplace transform of this function is

$$h_1(s) = 1/(s + 1)^2 + a\alpha/(s + \alpha)^2 \tag{44.2}$$

and clearly satisfies the high frequency requirements. The logic behind the design of H_1 is the fact that ue^{-u} is, for these purposes, a well behaved function and has a maximum at $u = 1$. H_1 as given in Equation (44.1) is a superposition of two such functions that have different maxima at different values of u, therefore making it likely that one can find values for u_0, a,

α such that $H_1'(u_0) = H_1''(u_0) = H_1'''(u_0) = 0$. This is indeed so and the values for u_0, a, and α are obtained from

$$u_0 = m + 1 + \sqrt{m + 1} \tag{45.1}$$

$$\alpha = m/\left(\sqrt{m + 1} + 1\right)^2 \tag{45.2}$$

$$a = \left(1/\sqrt{m} + \sqrt{1 + 1/m}\right)^{2(m + 1)} \cdot \exp\left(-2\sqrt{m + 1}\right) \tag{45.3}$$

by using m = 1, giving $u_0 = 3.41$; $\alpha = .17$; a = 2. Figure 11 shows a plot of this function with the peak amplitude normalized to 1. The quantity α is the ratio of the decay times and also the ratio of the cut off frequencies of the two contributors to Equation (44) and is, somewhat surprisingly, quite small. a is the ratio of the peak amplitudes of the two contributors to Equation (44.1) and a/α and $a \cdot \alpha$ control the magnitude of the second term in Equation (44.2) at small and large frequencies.

If the decay of H for large u is too slow to be acceptable, one could use procedures like mixing H subtractively with itself, but appropriately delayed and reduced in amplitude.

5.2) The Double Integrator

Before discussing double integrators that work, it is in order to describe at least one approach that in general does not work--using two identical single integrators in series. The reason is the following: While, during a certain length of time, the output of the first integrator gives a very good integral of the input, the second integrator integrates not only that part of the output signal, but also the part of the output that precedes the "good" part, thus giving erroneous signals.

The task of the double integrator is to deliver an accurate value of M_0 as defined by Equation (34) when not S_0 but $\dot{S}_0(t)$ is the input signal, with S_0 having the general properties ascribed to S_0 in Section 5.1.1.

With the input signal thusly defined, the output signal is given by

$$S_1(t) = \int_0^{T_1} \dot{S}_0(\tau)\, H(t-\tau)\, d\tau \quad .$$

For $t > T_1$, integration by parts gives

$$S_1(t) = \int_0^{T_1} S_0(\tau)\, \dot{H}(t-\tau)\, d\tau \quad . \tag{46}$$

This means that the whole content of Section 5.1.1 is directly applicable except one has to replace H by $\dot{H}$. However, designing $\dot{H}$ with the procedures given in Section 5.1 for H and then obtaining H by explicit integration of H is not proper in this context since it involves a perfect integration that one cannot do. Instead, the requirement that, for the same t, $H^{(m)} = 0$ for $m = 1, 2, 3$ has now to be satisfied for $m = 2, 3, 4$. It turns out that that is not more difficult than satisfying the conditions for the single integrator. As a model function, H and h as given by Equations (44) satisfy these conditions for $m = 2$ in Equations (45), yielding $u_0 = 4.7$, $\alpha = .27$; $a = 1.6$. Figure 12 shows, with normalized peak values, H_1 and $-H_1'$ according to this prescription. What is remarkable about this double integrator is the fact that one obtains the useful information from the part of H_1 that has a negative, nearly constant, slope <u>after</u> the maximum value of H_1. This response function is markedly different from the ideal function shown in Figure 9 and shows that it is the nearly constant slope of H_1 that counts, independent of what precedes it.

6) Closing Remarks and Acknowledgments

This somewhat long paper has been kept from being even longer by keeping out the description of many of the intermediate steps, such as the path to Equations (44) and (45), the Taylor series coefficient manipulation subroutines, the derivation of the specific forms of the reciprocity used here, etc. If a demand for these details develops, they will be made available in form of internal reports.

Writing this paper has greatly benefited from comments made by members of, and advisors to, the LBL BPM Team (P. Freda, D.A. Goldberg, J.A. Hinkson, D.E. Humphries, K.J. Kim, G.R. Lambertson, H.D. Lancaster, S.B. Magyary, S. Marks, E.H. Theil), by seminar audiences at LBL and SLAC, and by R.A. Shafer, LANL.

This work was supported by the Division of Advanced Energy Projects, U.S. Department of Energy, under Contract DE-AC03-76SF00098.

REFERENCES

1. J.H. Cuperus, Nucl. Inst. & Meth. 145, 219 (1977).

2. R.E. Shafer, IEEE Transactions on Nucl. Sci., NS-32, 1933 (1985).

3. R.H. Miller, J.E. Clendenin, M.B. James, J.C. Sheppard, Proceedings of the 12th International Conference on High-Energy Accelerators, 602 (1983).

4. In this paper, Z is used to indicate the Cartesian space coordinate in the direction of motion of the bunch, while x, y are the transverse Cartesian coordinates and $z = x + iy$.

Figure Captions

1) Coordinates Used to Describe Finite Size Beam
2) Hard Edge Charge Distribution in Rectangle
3) Hard Edge Distribution in Ellipse
4) Pick-Up Electrode Geometry
5) Charge on Pick-Up Electrode
6) MS Pick-Up Conductor in Duct
7) Geometry of Diamond-Shaped Duct with ES Pick-Up Electrodes
8) Map of Diamond-Shaped Disk onto Circular Disk
9) Ideal Response Functions for Single and Double Integrators
10) Static Part of Input Signal
11) Response Function for Single Integrator Model
12) Response Function for Double Integrator Model

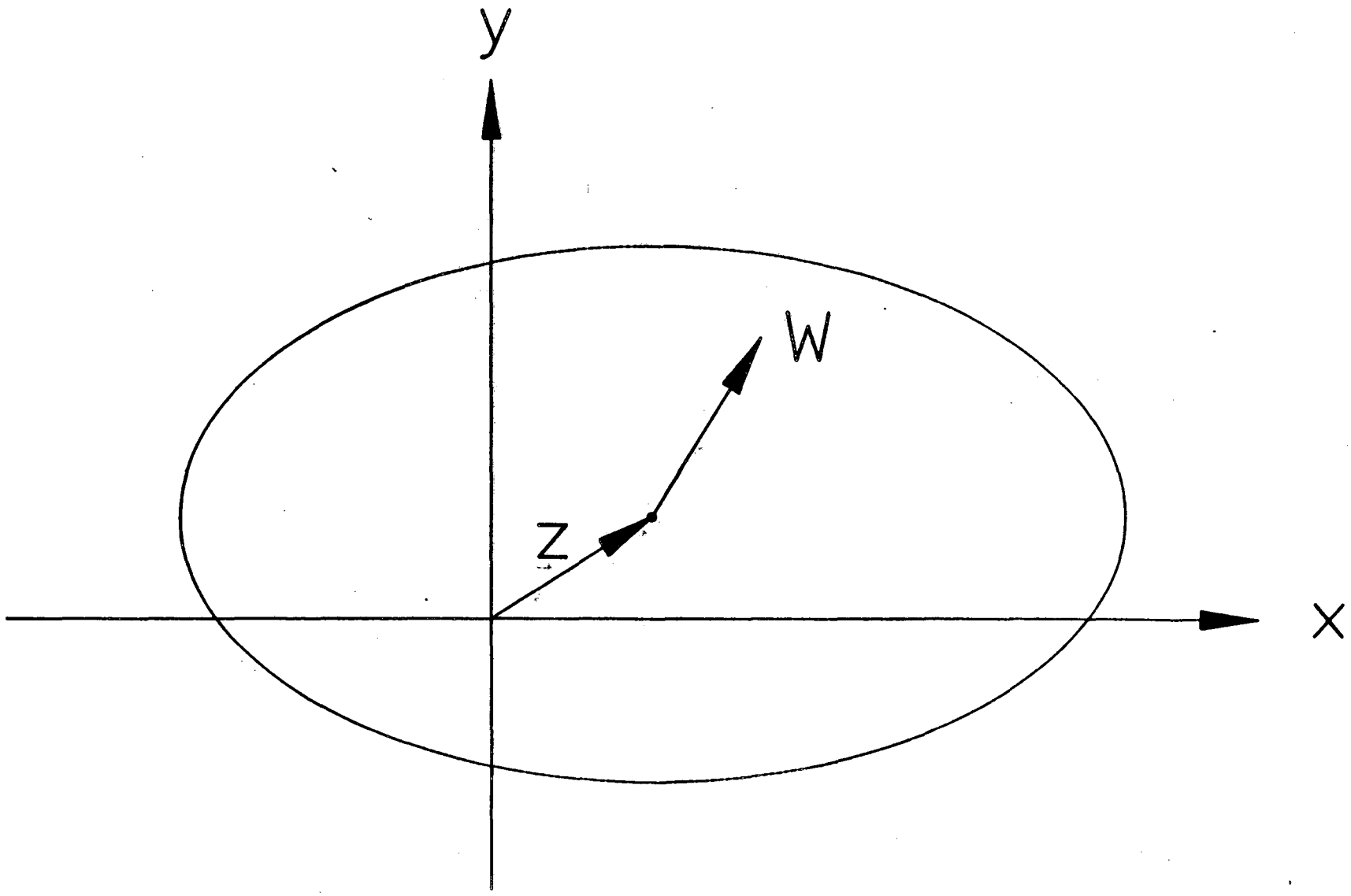

Figure 1

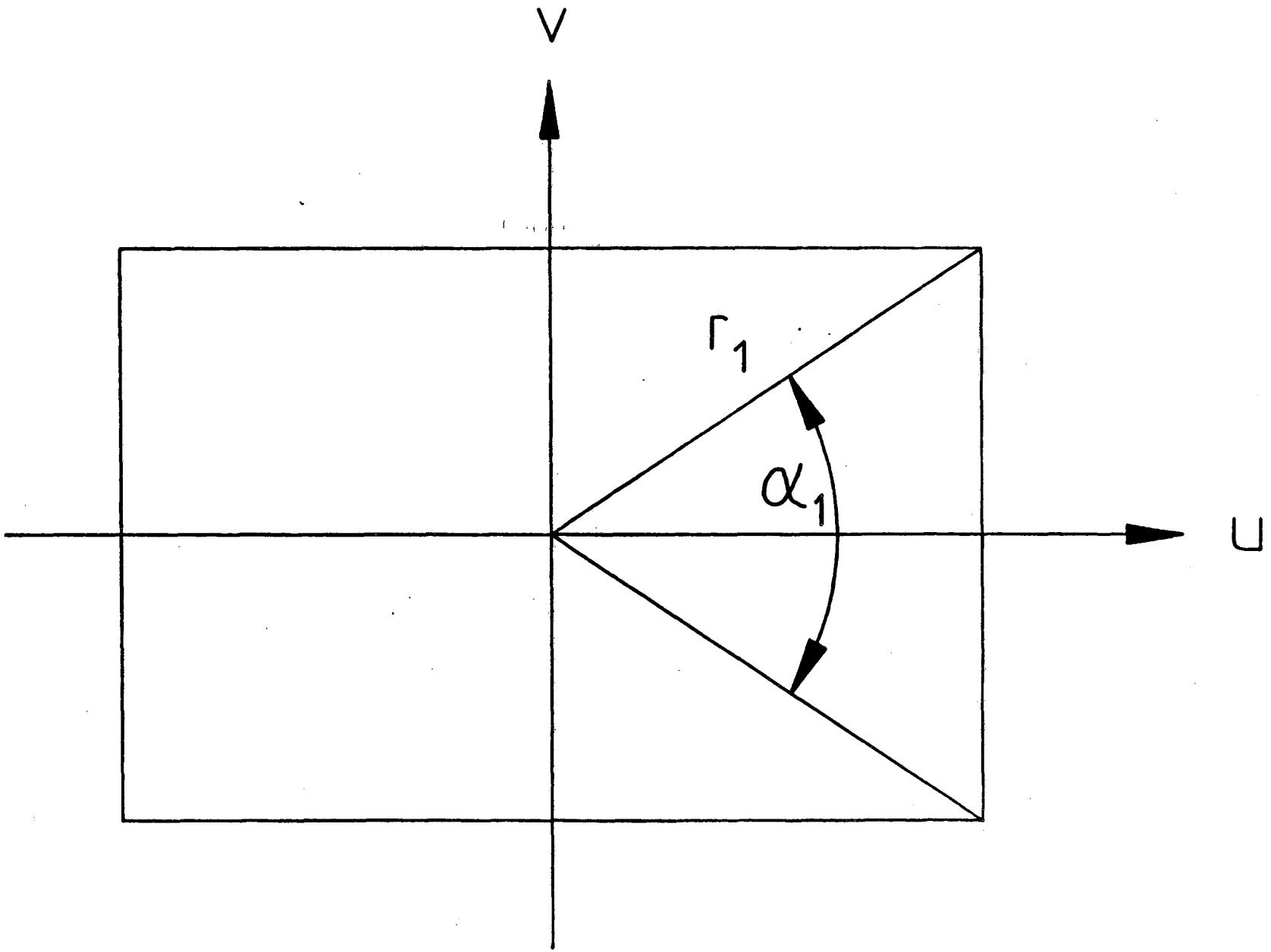

Figure 2

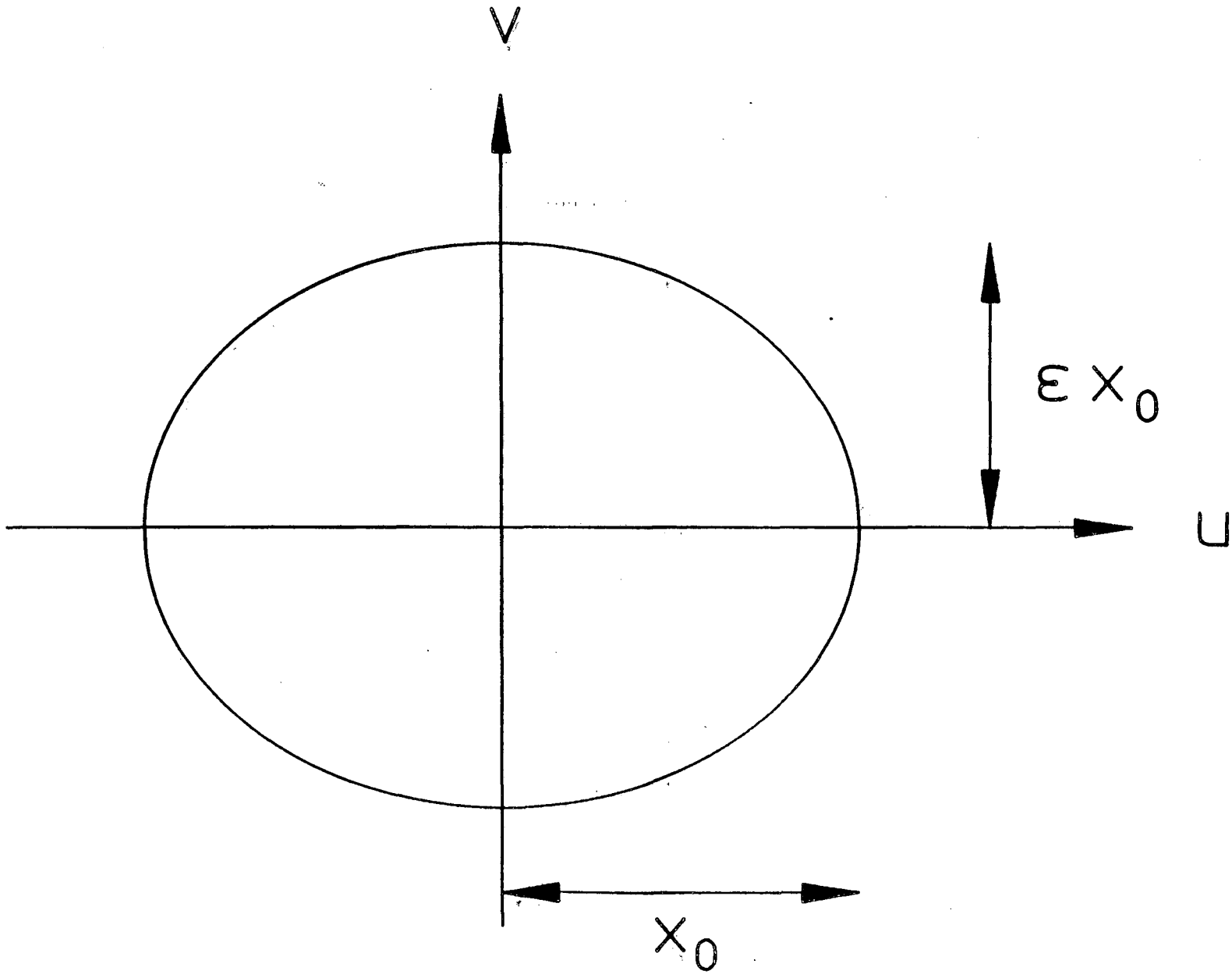

Figure 3

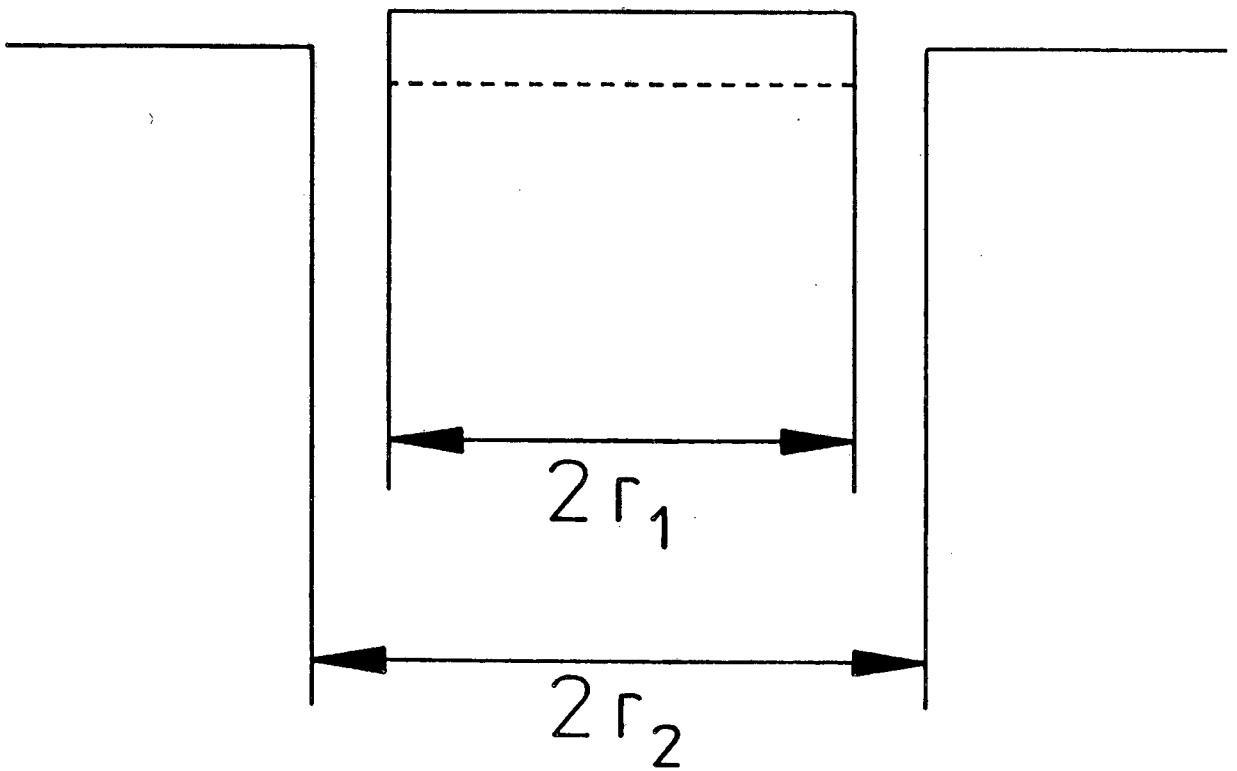

Figure 4

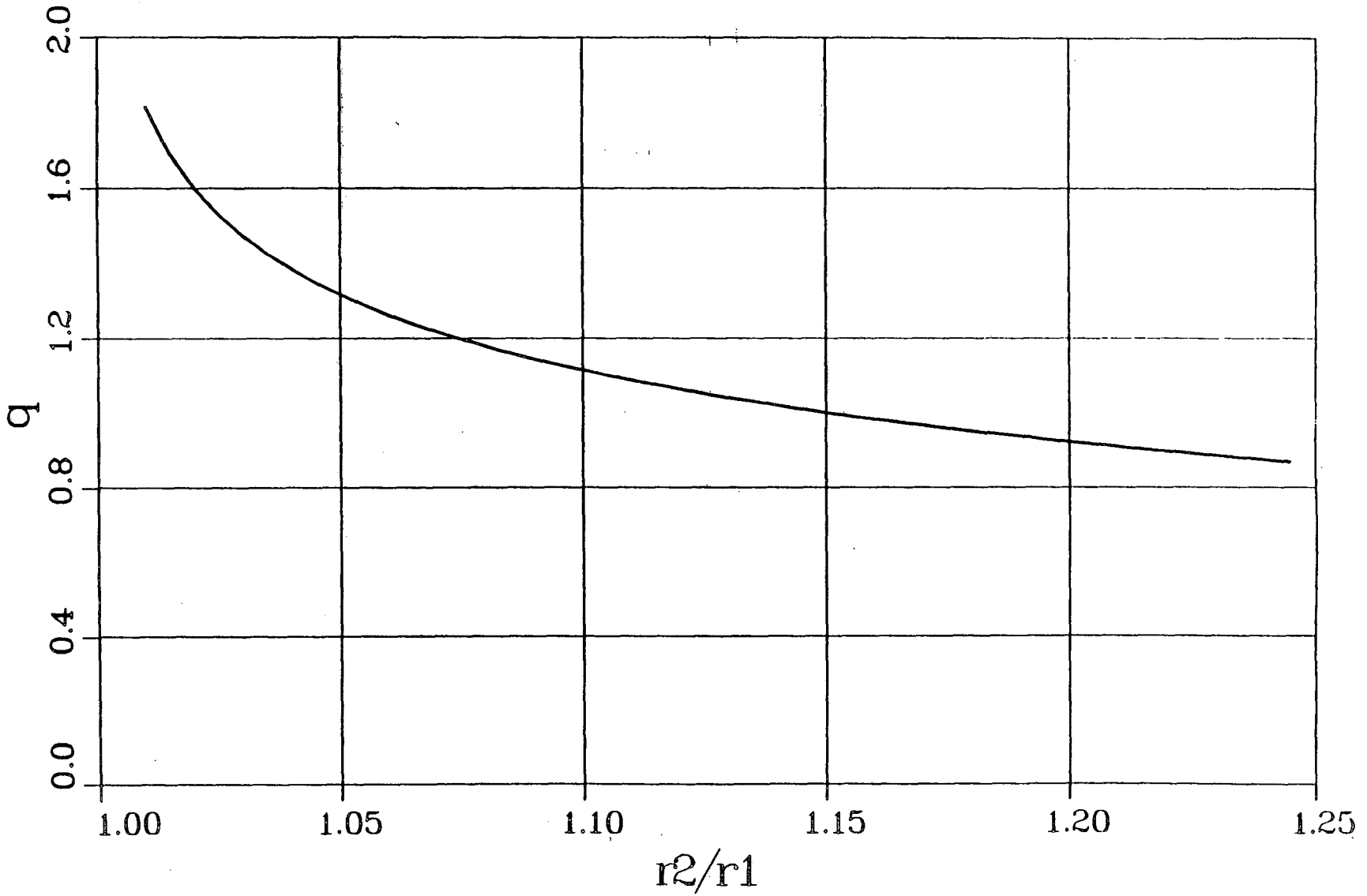

Figure 5

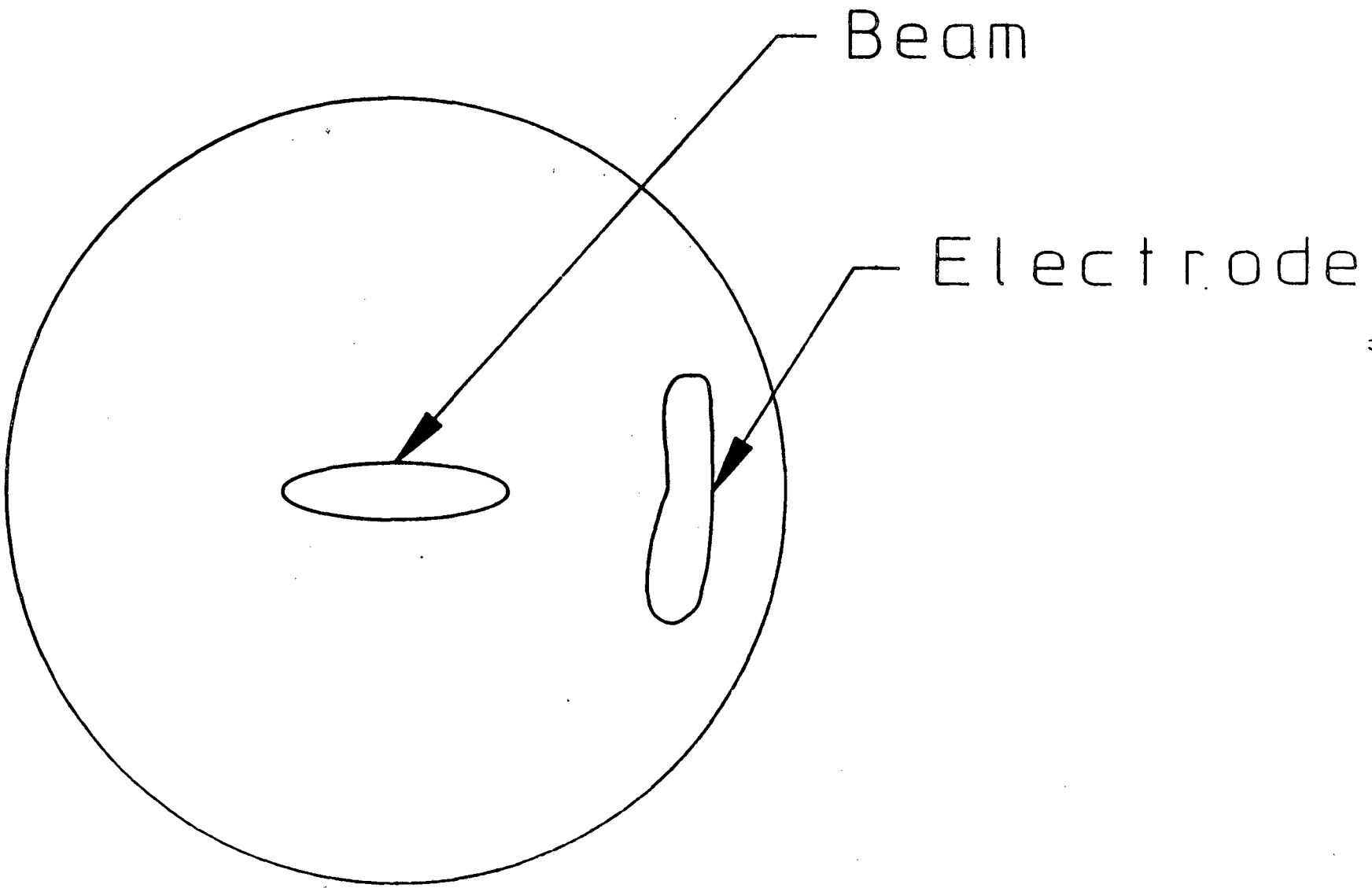

Figure 6

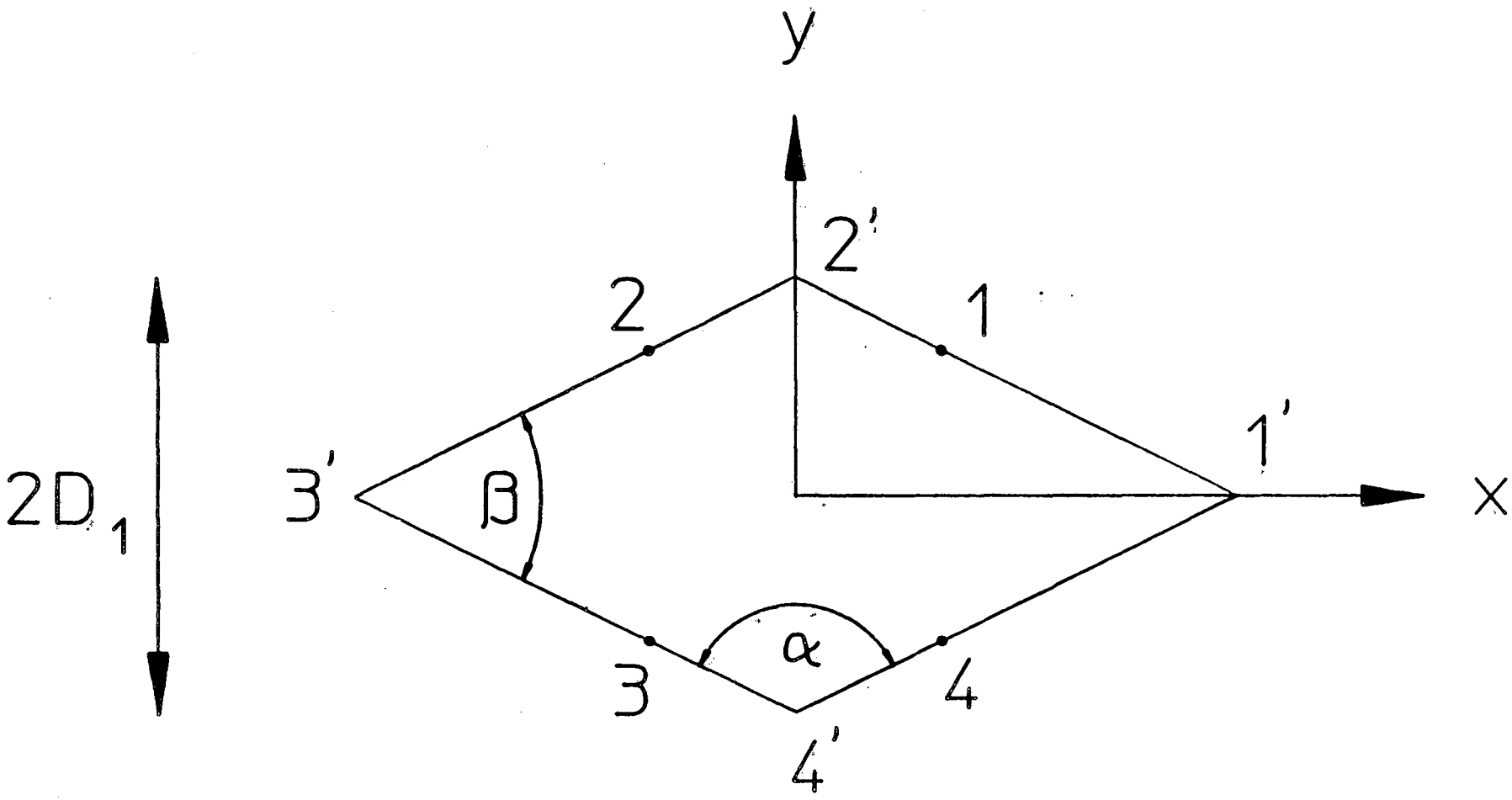

Figure 7

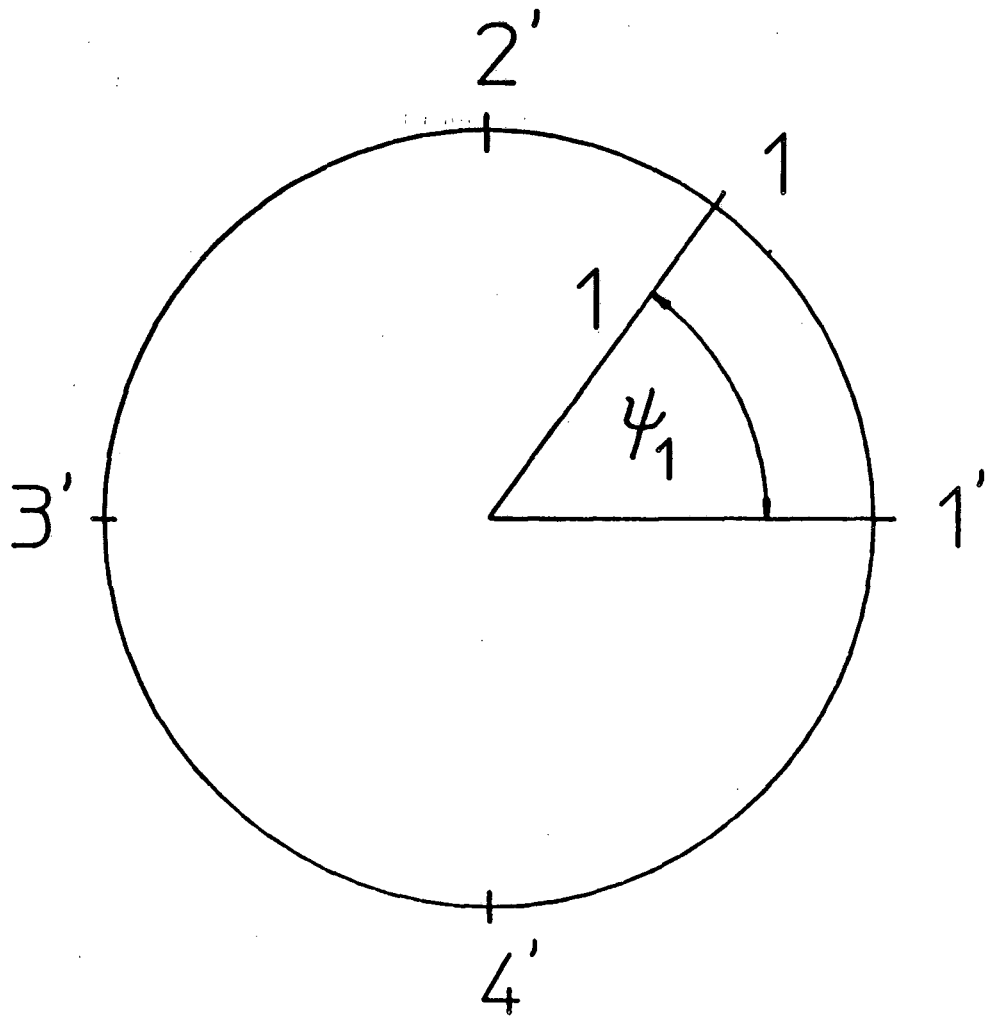

Figure 8

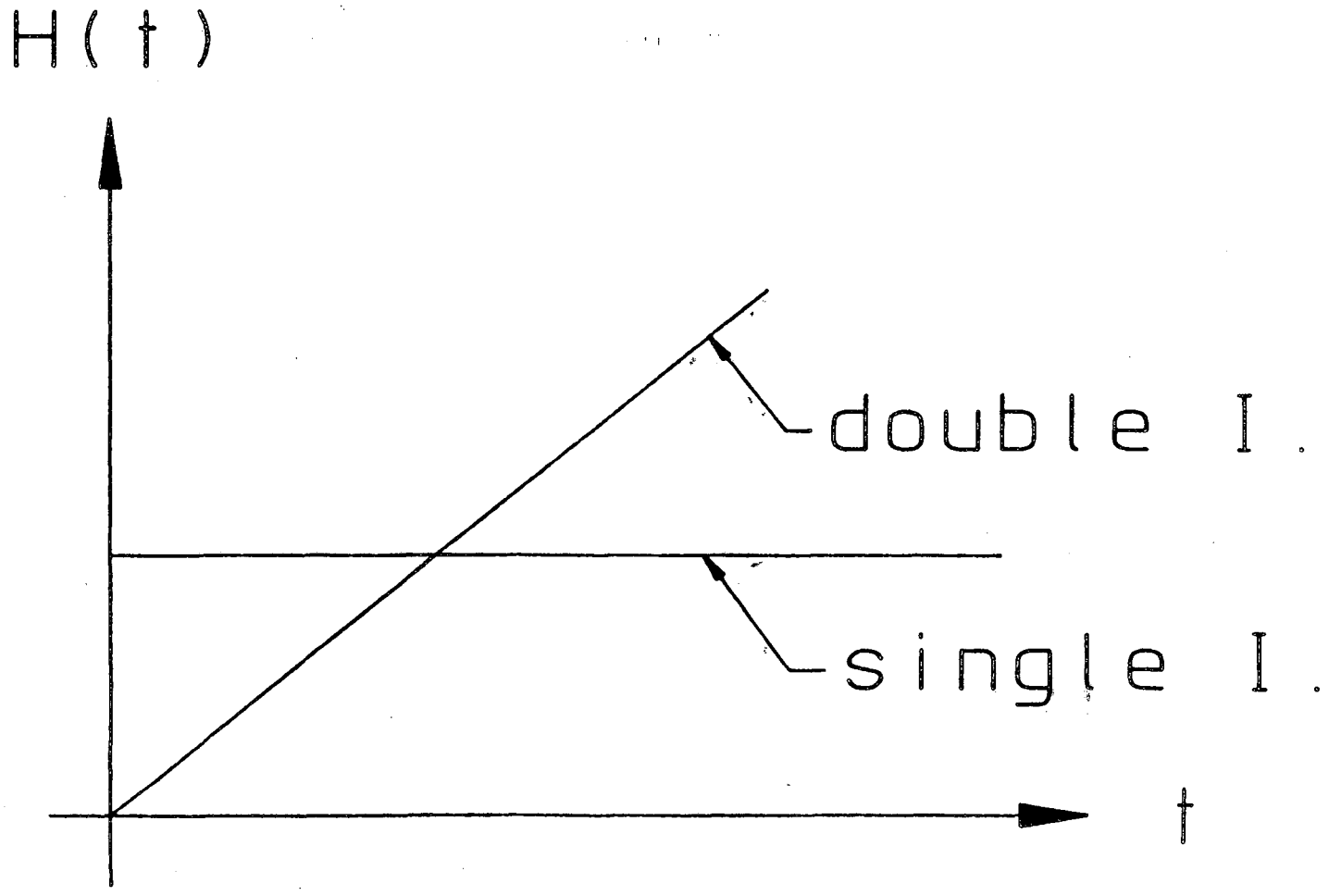

Figure 9

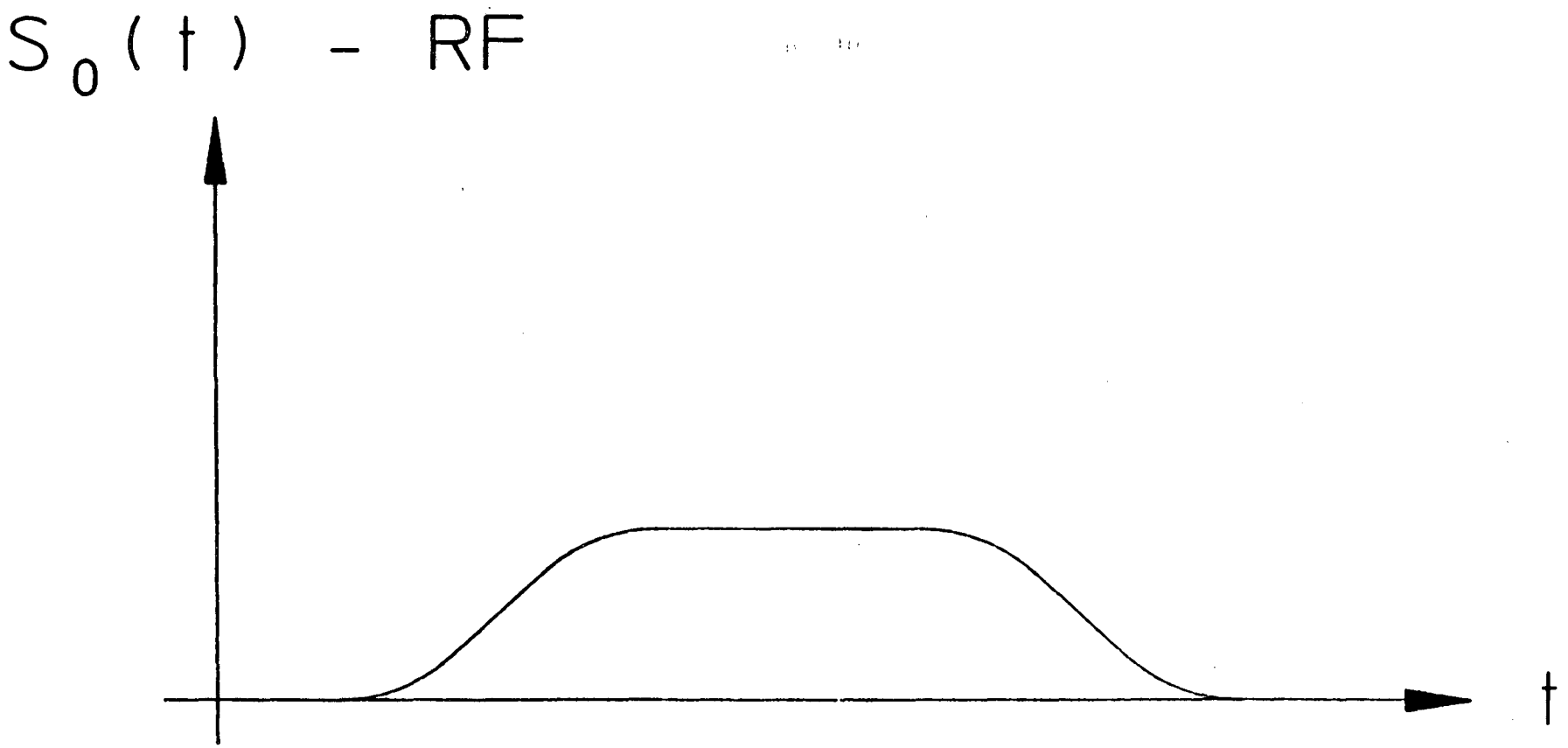

Figure 10

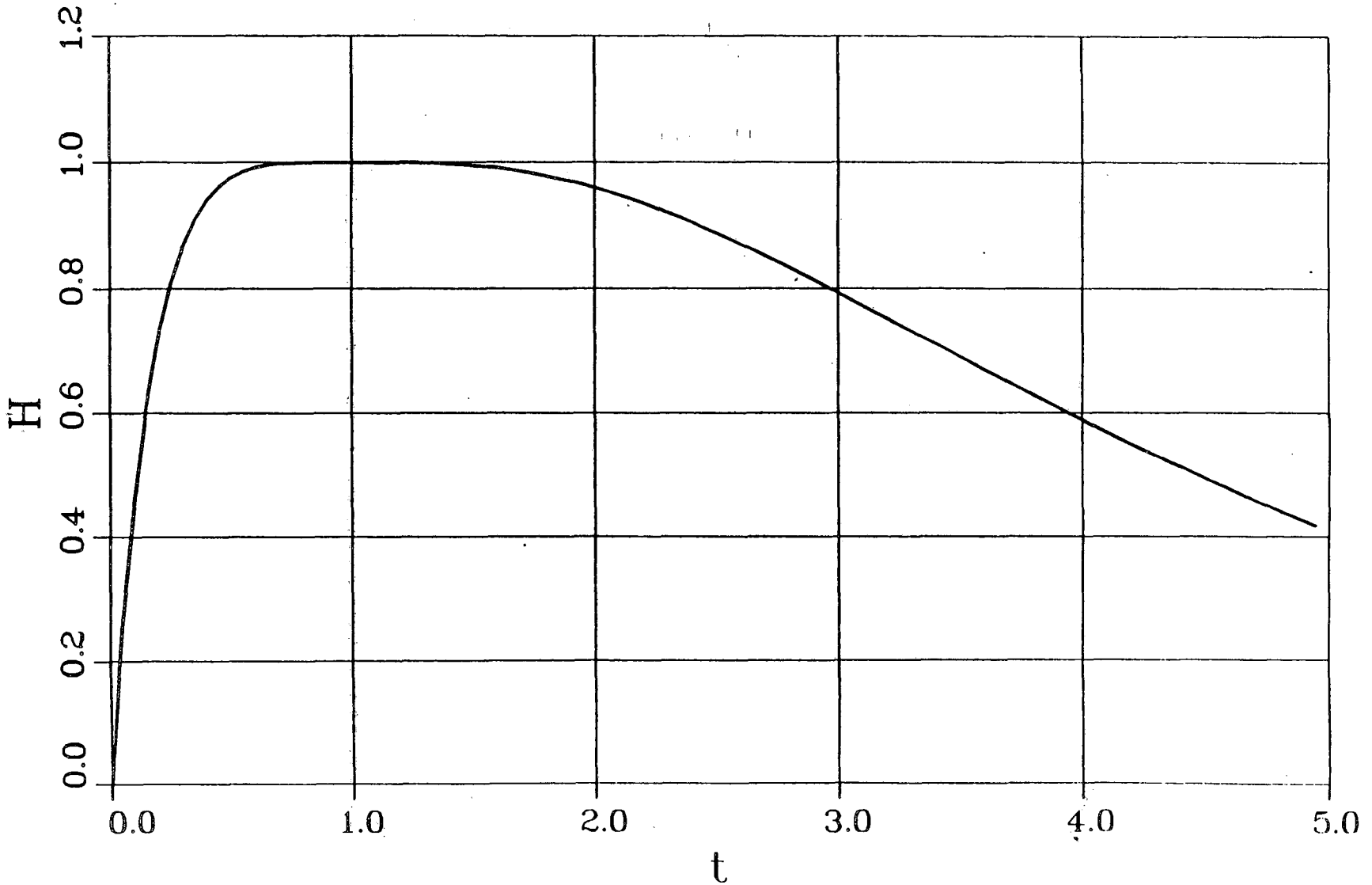

Figure 11

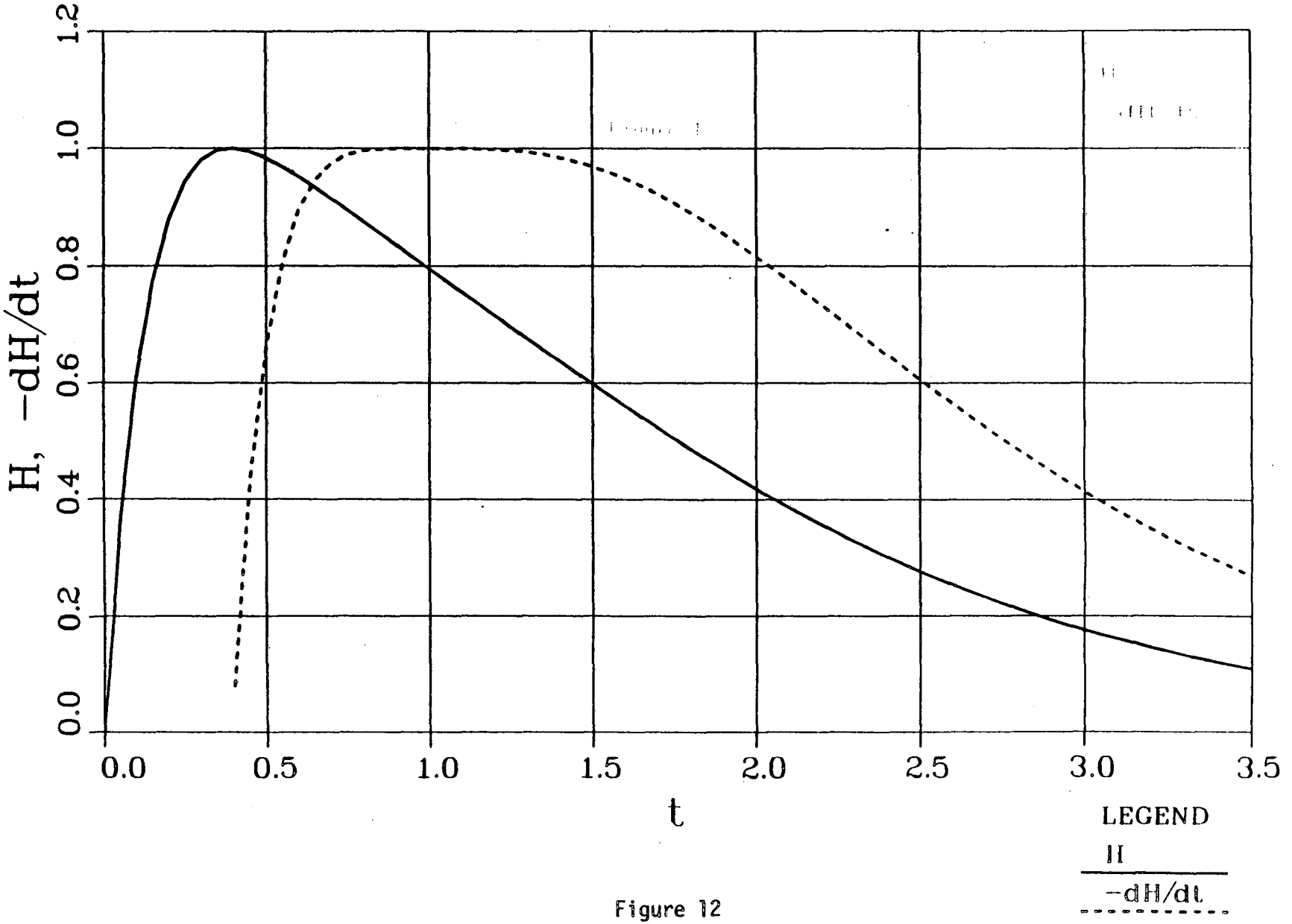

Figure 12

This report was done with support from the Department of Energy. Any conclusions or opinions expressed in this report represent solely those of the author(s) and not necessarily those of The Regents of the University of California, the Lawrence Berkeley Laboratory or the Department of Energy.

Reference to a company or product name does not imply approval or recommendation of the product by the University of California or the U.S. Department of Energy to the exclusion of others that may be suitable.

LAWRENCE BERKELEY LABORATORY
TECHNICAL INFORMATION DEPARTMENT
UNIVERSITY OF CALIFORNIA
BERKELEY, CALIFORNIA 94720